Magnon excitations in a mesoscopic Heisenberg ferromagnet

S. Cojocaru* and A. Ceulemans
Division of Quantum Chemistry, University of Leuven, Celestijnenlaan 200F, B-3001 Leuven, Belgium
(Received 24 June 2002; published 19 December 2002)

We report on a qualitative change of the character of interacting magnon excitations in a ferromagnet due to finite size. Within an improved continuum approach excitation modes are found analytically for a two-dimensional system. Several non-totally symmetric modes are obtained which were previously unknown. In contrast to excitations in one dimension some of the low energy modes approach the macroscopic limit extremely slowly. These modes occupy a substantial part of the Brillouin zone and can therefore be responsible for the logarithmic size dependence of various thermodynamic quantities.

DOI: 10.1103/PhysRevB.66.224416 PACS number(s): 75.50.Xx, 75.30.Ds

I. INTRODUCTION

The current interest in finite-size ferromagnets is due to progress in mesotechnology and nanotechnology devices involving spin degrees of freedom (see, e.g., Refs. 1–3). Some quantum Hall systems can be mapped onto a ferromagnetic model.[4] However, the transition from macroscopic to finite-size behavior[5] remains an open issue. The increased power of computer simulation methods has made relatively large clusters accessible for investigation, but general regularities of the excitation spectra are difficult to extract in this way. We develop an analytical approximation which captures finite-size effects and reveals interesting features in the excitation spectra. At first sight, one can hardly expect dramatic size effects in ferromagnets. For instance, the corrections to the thermodynamic limit due to finite N (the number of sites in one direction), predicted by the exact Bethe ansatz solution for the periodic Heisenberg spin-1/2 chain with isotropic nearest neighbor interaction[6] are found to be small and analytically converging for $N\rightarrow\infty$. An even faster convergence is anticipated for a higher dimensional lattice which can then be described within straightforward methods (see, e.g., Ref. 7). In the present paper we show that, in contrast to the traditional ways of thinking, finite size-corrections to excitation spectra in a two-dimensional (2D) system can be large and nonanalytical. Some new excitation modes are found to be responsible for a large share of the low energy spectrum and have a logarithmic size dependence. The approach builds upon a preliminary study[8] of the 1D system which allows comparison to the exact solution found by Bethe's ansatz.[6] We describe the distribution of two-magnon bound excitations over the Brillouin zone which reveals the general trends of multimagnon spectra mentioned above.

Our approach consists of a refinement of the commonly used continuum method in condensed matter, which becomes exact in the thermodynamic limit. Its main feature consists of the ''conservation'' of symmetries of the discrete lattice in the continuum wave function. Previous continuum treatments (see, e.g., Refs. 7,9–12) are apparently in agreement with the exact solution,[6] although, as mentioned by Mattis in Ref. 7, p. 155, the relation of Bethe's ansatz to the continuum approach is ''somewhat obscure.'' For instance, the single eigenenergy branch of the bound two-magnon state in one dimension coincides with Bethe's result for $N\rightarrow\infty$. However, even for the 1D case, the wave function has not been obtained explicitly within the continuum method and the point that, according to Bethe ansatz, there should be *two orthogonal* solutions, did not receive any attention. For higher dimensional lattices, where no exact results are available, it is predicted that there should be, e.g., two and three bound modes for the square and the simple cubic lattices, respectively. The symmetry classification of the excitation modes in the Brillouin zone is then considered *after* the continuum limit was taken (see, e.g., Ref. 13 for the 3D example). These issues might seem irrelevant since the finite-size correction to the excitation energies in the 1D case is at most $1/N^2$. This form of the finite-size correction is only reached at long wavelengths, i.e., for the inverse wave vector of the excitation $\sim\sqrt{N}$. It is a rather restricted region of the Brillouin zone where the so called string hypothesis breaks down.[14,15] Outside the critical region, i.e., for shorter wavelengths, the corrections become exponentially small, and therefore this hypothesis is successfully used to describe the thermodynamics of the Heisenberg chain. For higher dimensional lattices one naturally would expect that the corrections should become even less relevant. However, it is shown below that for a 2D lattice the analog of the critical region mentioned above becomes large and cannot be ignored. It will become clear that properties of the wave function are essential for this behavior and the construction of a proper continuum description requires that the symmetries of the wave function are explicitly taken into account. For instance, we recover the ''lost'' second mode of Bethe's exact solution for the chain, and reveal four additional bound modes for the square lattice. The new modes in higher dimensions turn out to be ''genealogically'' related to Bethe's second mode. The distribution of the two-magnon states over the Brillouin zone shows that these modes outnumber the ones already known. It is clear that the same features are present in multimagnon spectra.

II. CONTINUATION OF THE BIMAGNON EQUATIONS

We first show how the main properties of the Bethe's exact solution can be described within the framework of our continuum approach for the $S=1/2$ Heisenberg Hamiltonian,

$$\hat{H}=-\sum_{\langle i,j\rangle} J_{ij}\mathbf{S}_i\cdot\mathbf{S}_j,$$

where $J_{ij}=J>0$ for the z nearest neighbors, and zero otherwise. Since the total momentum of the excitation $\mathbf{P}$ is a conserved quantity, it is convenient to consider the amplitude of the two magnon excitation $\Psi(\mathbf{n}_1,\mathbf{n}_2)$ in terms of the ''center of mass'' $\mathbf{R}$ and relative $\mathbf{r}$ coordinates of the flipped spins, $R_x=(n_2^x+n_1^x)/2$, $r_x=(n_2^x-n_1^x)$, etc. Thus, up to a constant factor, for the amplitude we have

$$\Psi(\mathbf{n}_1,\mathbf{n}_2)=\exp(i\mathbf{P}\cdot\mathbf{R})a(\mathbf{P}|\mathbf{r}). \tag{1}$$

The Schrödinger equation takes the form[7]

$$[\varepsilon-zJ]a(\mathbf{P}|\mathbf{r})+J\sum_{\mathbf{d}}\cos\left(\frac{\mathbf{P}\cdot\mathbf{d}}{2}\right)a(\mathbf{P}|\mathbf{r}+\mathbf{d})=J(\mathbf{r})\times\left[a(\mathbf{P}|\mathbf{0})\cos\left(\frac{\mathbf{P}\cdot\mathbf{r}}{2}\right)-a(\mathbf{P}|\mathbf{r})\right], \tag{2}$$

where ε is the excitation energy, the sum runs over the nearest neighbors and $J(\mathbf{r})=J_{ij}$. In the following energy is assumed to be in units of J. Some symmetry requirements follow from permutation of overturned spins $[a(\mathbf{P}|\mathbf{r})=a(\mathbf{P}|-\mathbf{r})]$ and from cyclic boundary conditions $[\Psi(n_1^x,n_1^y;n_2^x,n_2^y)=\Psi(n_1^x,n_1^y;n_2^x+N,n_2^y)=\Psi(n_1^x+N,n_1^y;n_2^x,n_2^y)=\Psi(n_1^x,n_1^y+N;n_2^x,n_2^y)$, etc.]:

$$a(\mathbf{P}|r_x,r_y)=\exp\left(\frac{iP_xN}{2}\right)a(\mathbf{P}|N+r_x,r_y)=\exp\left(\frac{iP_xN}{2}\right)a(\mathbf{P}|N-r_x,r_y)\ldots\ . \tag{3}$$

We adopt Bethe's convention of numbering the lattice sites, so that the relative coordinates $r_x(=X)$ and $r_y(=Y)$ are nonnegative integers on the main interval: $X=0,1,\cdots,N-1$ for the chain and $X=0,1,\cdots,N-1$ and $Y=0,1,\cdots,N-1$ for the square lattice. By these definition one has the following coordinates for the nearest neighbors on the 1D lattice: $X=1$ and $X=N-1$ instead of the usual $X=-1$. The advantage of this choice is that it includes the boundary conditions in an explicit form, e.g., it allows for the amplitudes on nearest neighbor sites $[a(P|1)$ and $a(P|N-1)]$ to have *different* signs in agreement with Eq. (3). The usual choice $X=-1$, although being correct for the even parity states (see below), is generally misleading since, e.g., in one dimension it in fact represents the transposition of flipped spins and not the true dynamics on the lattice. The cyclic boundary conditions imply that the relative motion of flipped spins has a period $2N$. In a similar way multiple periods of N would arise in the relative amplitude for multimagnon states. The above arguments will become important for the discussion of the modes which are intrinsically related to Bethe's second mode in one dimension: The nearest neighbors for the square lattice are defined by analogy with one dimension: $(X=1,Y=0)$, $(X=0,Y=1)$, $(X=N-1,Y=0)$, and $(X=0,Y=N-1)$. The components of the total momentum take on the values $2\pi l_x/N$ and $2\pi l_y/N$, where l_x and l_y are integer quantum numbers. The existence of two-particle eigenstates with even and odd parity immediately follows from Eq. (3) depending on the parity of l. We then expand the amplitude of the relative motion into the Fourier series

$$a(\mathbf{P}|\mathbf{r})=\frac{1}{N^2}\sum_{\mathbf{Q}}b(\mathbf{P}|\mathbf{Q})\cos(\mathbf{r}\cdot\mathbf{Q}). \tag{4}$$

The constraints on the variable $\mathbf{Q}$ in Eq. (4) imposed by Eq. (3) imply that

$$\exp\left[iN\left(\frac{P_{x,y}}{2}\pm Q_{x,y}\right)\right]=1.$$

This relation determines the range of values for the respective components of $\mathbf{Q}$:

$$Q_{x,y}^s=\frac{2\pi m}{N},\quad Q_{x,y}^a=\frac{2\pi m}{N}+\frac{\pi}{N},\quad m=0,1,\ldots,N-1. \tag{5}$$

The Fourier amplitude $b(\mathbf{P}|\mathbf{Q})$ and the eigenenergy ε are then obtained as solutions of Eq. (2). As our aim is to construct a continuum approximation which would keep track of the major properties of the underlying finite lattice, it has to incorporate the symmetry related shift π/N in Eq. (5). Therefore we replace the sums by integrals, as required by continuum approach, *but the integration interval is shifted in momentum space*,[8] i.e.,

$$\frac{1}{N}\sum_{Q^a}\rightarrow\frac{1}{\pi}\int_{\pi/N}^{\pi+\pi/N}dQ. \tag{6}$$

The above approximation can be viewed as a truncation of the Euler-MacLaurin expansion (see, e.g., Ref. 16), Chap. 4. In Eq. (6) we keep the main term of the expansion. The bounds of the integral correspond to the half of the total integration interval which is accounted for by the trivial factor 2 (see Ref. 8). The advantage of using the periodic functions of the Fourier series [Eq. (4)] consists of the cancelation of terms containing derivatives of the integrand in Euler-MacLaurin expansion (see Eq. 4.19 in Ref. 16). Thus the remainder of such a truncation giving an estimate of the accuracy of the approximation (6) is $1/N^2$. However, as is shown in Chap. 5 of Ref. 16 the accuracy is actually even higher. Such accuracy is sufficient for the purpose of our approximation, which is meant to capture the main terms of the finite-size correction, because as it will become clear from the following the actual values of the integrals are finite, i.e., $\sim O(1)$. We point out that the shift occurs because of the boundary conditions. Other boundary conditions would result in a different shift which should be incorporated in a similar way. In one dimension for such a continuum approximation we indeed obtain two different branches, symmetric (s) and antisymmetric (a), in agreement with Bethe's solution. The proper analytical continuation from a discrete lattice is achieved by explicitly introducing the symmetry requirements into the amplitude:

$$A_{s,a}(p|x)=\frac{1}{2}[a_{s,a}(p|x)\pm a_{s,a}(p|N-x)]. \tag{7}$$

The corresponding Fourier amplitudes are $b_{s,a}(Q)\sim\cos Q\times[\cos v_{s,a}-\cos Q]^{-1}$, where $\cosh v_{s,a}\equiv(1-\varepsilon_{s,a}/2)/\cos(p/2)$ and p is a continuous variable, the counterpart of the total

momentum **P**. Normalization constants are then readily obtained and we obtain the correct result which coincides with the Bethe ansatz for $N\to\infty$:

$$A_{s,a}(p|x)=\sin\left(\frac{p}{2}\right)/\sqrt{2}\left[\cos^{x-1}\left(\frac{p}{2}\right)\pm\cos^{N-x-1}\left(\frac{p}{2}\right)\right].$$

The single branch mentioned above (see, e.g., Refs. 7 and 10) corresponds to the symmetric solution $\varepsilon_s=\sin^2(p/2)$, while the antisymmetric branch is described by the equation

$$1-\frac{2}{\pi}\frac{\sin\left(\frac{\pi}{N}\right)}{\cosh v_a}=\frac{2[\cosh v_a-\cos(p/2)]}{\pi\sinh v_a}\arctan\left(\frac{\sinh v_a}{\sin\left(\frac{\pi}{N}\right)}\right). \tag{8}$$

As shown earlier, our approximation reproduces well the exact solution also at finite N (see Ref. 8 for a more detailed discussion). It displays the correct behavior at the border of the Brillouin zone: $\varepsilon_a=\varepsilon_s=1$. Toward the long-wavelength region the energy of the antisymmetric excitation grows higher than that of the symmetric one, their separation being scaled as p^4 for small momenta. Both branches lie below the continuum of scattered magnon states until the latter is crossed by $\varepsilon_a(p)$ at some critical momentum $p_c\simeq 2\pi/\sqrt{N}$ which should be compared to the exact value found by Bethe $P_c^B\simeq 4/\sqrt{N}$. From Eq. (8) one can see that it predicts a continuous real valued solution for the eigenenergy beyond the crossing point, in the region of scattered states, $\varepsilon_a>2J[1-\cos(p/2)]$. This might seem to be in contradiction with Bethe's solution, which predicts that the bound state exists only below the region of scattered states. However, upon a closer look, one should recognize in v the imaginary part of Bethe's phase, $\theta=iv$. Then it is clear that at the crossing point $v=0$ Eq. (8) describes the ''dissociation'' of the bound state (real v, or a localized wave function) into scattered magnons (imaginary v, or an oscillating wave function). The physical reason for the instability of the antisymmetric bound state is the vanishing of magnon attraction at the crossing point both exactly and in our approximation. Although for a finite lattice only discrete momenta have physical meaning, the continuous variables in our approach should be considered in the interpolation sense, precisely as the Bethe ansatz transcendental equations for the finite chain. Indeed, one can check that Bethe's equations describe the same crossover behavior. Thus there is no coexistence of bound and scattered states below the critical momentum, and the transition is characterized by the qualitative change of the wave function: the phase variable v becomes purely imaginary above the crossing point. It should be stressed that, as is generally the case for a continuum treatment, Eq. (8) cannot be used for a quantitative description of the scattering magnon region by mere analytical continuation in v. The equation for the Fourier amplitude should take into account the dense energy spacing ($\sim 1/N$) of scattering solutions according to the standard procedure (see, e.g., Ref. 7, Chap. 5.3) and can be considered in our approach as well. This is, however, beyond the scope of the present paper. We note that for the Bethe ansatz equations the $1/N$ expansion was considered before, and in the longwave region $P\lesssim 1/\sqrt{N}$ of the spectrum nonstring solutions were obtained,[14,15] which can be identified as the true solutions of Bethe's equations. In contrast to the string solutions which are valid for higher momenta and unite odd and even branches, only the even symmetry state was shown to exist in the longwave region. The behavior described by our approximation agrees well with the above picture, but quantitatively it of course slightly deviates from the exact asymptotic expansion.[8]

III. TWO-MAGNON PROBLEM ON A SQUARE LATTICE

For the two-magnon problem on the square lattice the solution first obtained by Wortis[10] predicted two energy branches. As already noted, by ignoring the unusual size dependence of some modes, this treatment has largely overlooked the rich structure of the spectrum in the mesoscopic to even macroscopic range. To identify the different types of excitations one should carefully apply symmetry relations (3) depending on the parity of the quantum numbers l_x and l_y and also the symmetry group C_{4v} of the lattice. The excitation modes must transform according to the irreducible representations of the group. Their classification is obtained by using the projection operator $\hat{O}_\alpha$ (see, e.g., Ref. 17). The action of $\hat{O}_\alpha$ on Fourier expansion (4) projects out a function which transforms according to one of the five irreducible representations α of the group: four one-dimensional representations A_1, A_2, B_1, and B_2 and one two-dimensional representation E. There are three different combinations of the quantum numbers: (1) both l_x and l_y are even, (2) both l_x and l_y are odd, and (3) the numbers are of different parity. These combinations determine the respective sequences for **Q** in Eq. (4). The projection operator then generates the modes allowed for a particular combination by applying the group transformations. The same can be achieved by applying first the ''filter'' of rotational symmetry and then determine the quantum numbers compatible with the respective mode (Appendix A). Thus for the one-dimensional representations we find

$$\begin{aligned}
&b_{A_1}(P_x,P_y|Q_x,Q_y)=b_{A_1}(P_y,P_x|Q_y,Q_x),\ \{P_x,P_y\}\ \text{even},\\
&b_{B_2}(P_x,P_y|Q_x,Q_y)=b_{B_2}(P_y,P_x|Q_y,Q_x),\ \{P_x,P_y\}\ \text{odd},\\
&b_{B_1}(P_x,P_y|Q_x,Q_y)=-b_{B_1}(P_y,P_x|Q_y,Q_x),\ \{P_x,P_y\}\ \text{even},\\
&b_{A_2}(P_x,P_y|Q_x,Q_y)=-b_{A_2}(P_y,P_x|Q_y,Q_x),\ \{P_x,P_y\}\ \text{odd}.
\end{aligned} \tag{9}$$

The remaining values of the total momentum correspond to the two components of the E mode: $A_E^y(P_x,P_y|X,Y)$ has P_x *even*, and P_y *odd*, and $A_E^x(P_x,P_y|X,Y)$ has P_y *even* and P_x *odd*. The symmetry analysis demonstrates that parity of the quantum numbers of the total momentum determine the type of mode which can be excited for the particular value of **P**. The energy of each mode is obtained by solving the Schrödinger equation for the irreducible amplitude. Then the respective Fourier component is obtained up to a constant fac-

tor which is determined from the normalization condition. The analytic continuation must be carried out for the symmetrized quantities in analogy with Eq. (7), and the finite sums are replaced by integrals according to Eq. (6). To simplify the discussion, let us consider the diagonal direction in the Brillouin zone $P=P_x=P_y$. Then for the excitation with both even components of **P** we recover the two energy branches found by Wortis. However, due to the symmetry filtering, instead of the factorized form for the 2×2 matrix of the eigenenergy equation (52) in Ref. 10 we obtain two separate equations depending on the symmetry of the mode. This then allows us to identify the two modes as A_1 (s wave), the lowest energy mode, and B_1 ($d_{x^2-y^2}$), the highest energy mode. The A_1 mode (Fig. 1) has the usual shape of a localized wave function with the periodicity of the original lattice. However, unlike the total wave function [Eq. (1)], the relative amplitude [Eq. (4)] is generally not required to have the periodicity of the original lattice (see, e.g., Ref. 8) and for the two-magnon case can be antiperiodic. Indeed, if at least one quantum number of the excitation is an odd integer, then the relative amplitude becomes antisymmetric in the direction of the respective component of **P**, e.g., $a(X,0)=-a(X,N)\neq 0$ if l_y *odd* ($P_y=2\pi l_y/N$). This allows for a nonzero value of the amplitude on the nearest neighbor sites, $a(1,0)\neq 0$, for such modes as B_2 and A_2 as shown in Appendix A. Therefore, for such momenta the B_2 mode, for example, cannot be identified with the transformation properties of the ''molecular'' function d_{xy} which has $a(1,0)=0$. This feature is a direct consequence of the lattice symmetry and the boundary conditions. The identification mentioned above is possible for the even parity quantum numbers, but then for our square lattice with nearest neighbor interaction

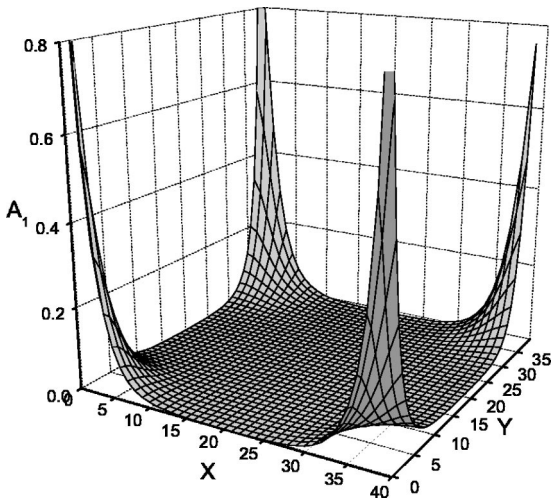

FIG. 1. The amplitude of the A_1 mode along the diagonal direction $p_x=p_y$ for the 40×40 square lattice. This result corresponds to the solution found in Ref. 10.

the amplitude is identically zero. Since the magnon interaction represented by the right-hand side of Eq. (2) has a local character and depends only on nearest neighbors the nonzero value of the amplitudes means that for odd quantum numbers the spin waves are allowed to interact, and therefore a bound state becomes possible. It turns out that such ''antisymmetric'' states are responsible for logarithmic size dependencies in two dimensions.

Let us now consider the behavior of the B_2 and A_2 modes along the diagonal direction in the Brillouin zone. After symmetry projection from Eq. (2) we obtain

$$A_{B_2(A_2)}(X,Y)=\frac{F_{A_2(B_2)}}{N^2}\sum_{Q_x^a,Q_y^a}\frac{[\cos(Q_x^a)\pm\cos(Q_y^a)]\cos(Q_x^aX+Q_y^aY)}{2-\varepsilon/2-\cos\left(\frac{P_x}{2}\right)\cos(Q_x^a)-\cos\left(\frac{P_y}{2}\right)\cos(Q_y^a)}, \tag{10}$$

where ''+'' stands for the B_2 mode, and

$$F_{B_2(A_2)}(P_x,P_y)=\frac{1}{N^2}\sum_{Q_x^a,Q_y^a}b_{B_2(A_2)}(Q_x^a,Q_y^a)\left[\cos\left(\frac{P}{2}\right)-\cos(Q_x^a)\right].$$

The corresponding eigenenergies ε are found as solutions of the compatibility equation

$$1+2A(P)\cos\left(\frac{P}{2}\right)-B(P)-C(P)=0 \tag{11}$$

for the B_2 mode and

$$1-B(P)+C(P)=0 \tag{12}$$

for the A_2 mode, respectively. In the continuum representation the sums

$$A(P)=\frac{1}{N^2}\sum_{Q_x^a,Q_y^a}\frac{\cos(Q_x^a)}{2-\cos\left(\frac{P}{2}\right)[\cos(Q_x^a)+\cos(Q_y^a)]-\varepsilon/2},$$

$$B(P)=\frac{1}{N^2}\sum_{Q_x^a,Q_y^a}\frac{\cos^2(Q_x^a)}{2-\cos\left(\frac{P}{2}\right)[\cos(Q_x^a)+\cos(Q_y^a)]-\varepsilon/2}, \tag{13}$$

$$C(P)=\frac{1}{N^2}\sum_{Q_x^a,Q_y^a}\frac{\cos(Q_x)\cos(Q_y)}{2-\cos\left(\frac{P}{2}\right)[\cos(Q_x^a)+\cos(Q_y^a)]-\varepsilon/2}$$

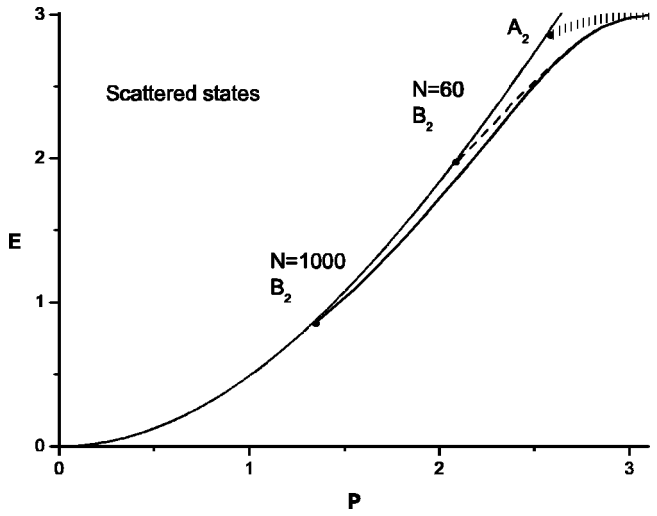

FIG. 2. The dispersions of the two antisymmetric bound modes A_2 (the highest curve with vertical dashes representing a very weak N dependence) and B_2 for $N=60$ (dashed line) and $N=1000$ (lower continuous line) as determined by the refined continuum solution of Eq. (2). The curves terminate at the respective crossing points with the boundary of scattered states (upper continuous line). The energy of the B_2 mode decreases with the increase of N. The dispersion of the A_1 mode (not shown) lies lower and terminates at $p=0$. Note that the number of lattice points corresponds to N^2.

are replaced by integrals which can either be expanded in asymptotic series or calculated numerically. Equations (11) and (12) coincide with the respective equations for the A_1 and B_1 modes in the limit $N\rightarrow\infty$. For some mesoscopic values of N both dispersions are shown in Fig. 2. The A_2 mode has small N corrections, and its dispersion follows that of the B_1 mode, while the B_2 mode, on the contrary, has large size corrections and for any finite N is well separated from all the other modes. Two different branches are also obtained for each component of the E mode. The low energy branch (E^l) closely follows that of the B_2 mode but lies slightly lower, while the high energy branch (E^h) almost coincides with that of the A_2 mode. Note that for the E mode the ''diagonal direction'' of the total momentum in the Brillouin zone is not allowed due to the mixed set of quantum numbers and has to be understood in an approximate sense. For an arbitrary direction the equations become more involved but the qualitative picture of the six eigenenergy branches outlined above remains unchanged. One can easily see that all the modes become degenerate close to the corner of the Brillouin zone with energy $3J$, the two flipped spins are tightly bound and propagate through the lattice preserving the nearest neighbor location. A ''one-dimensional'' behavior is realized at the edges of the Brillouin zone, when dispersion is possible only in one of the directions. However, the symmetry related properties of the excitations appear most prominently at low energies and long wavelengths where some of the modes become unstable toward decay into scattered magnons. This takes place at the crossing line with the boundary of scattered excitations, $E_L=2[2-\cos(p_x/2)-\cos(p_y/2)]$, in analogy with the 1D problem. The high energy modes (A_2, B_1, and E^h) have a very narrow and anisotropic region of stability and become unstable at almost the same critical line at high momenta. From the asymptotic expansion of Eq. (13) (see Appendix B), after substitution in Eq. (12) we find the same critical momentum p_c as obtained by Wortis with insignificant size corrections $p_c \simeq 2\arccos[(4/\pi)-1]+O(1/N)$. For the B_2 mode the main terms of the asymptotic expansions do not cancel in eigenenergy equation (11) and the critical point becomes dependent on $\ln N$:

$$2\left[1-\cos\left(\frac{p^c_{B_2}}{2}\right)\right]\simeq\frac{1}{\frac{1}{\pi}\ln N-0.22}. \tag{14}$$

In a similar way, for the low energy component E^l one obtains

$$2\left[1-\cos\left(\frac{p^c_{E}}{2}\right)\right]\simeq\frac{1}{\frac{1}{\pi}\ln N-0.16}.$$

The critical line $\varepsilon=E_L(p_x,p_y)$ is obtained by changing the direction of $\mathbf{p}$. The respective asymptotic expansions are more complicated and will not be given here. However, for the leading term a simple expression can be obtained for the integrals involved in the eigenenergy equation (see Appendix B). If at least one of the integrals contains a low energy cutoff corresponding to the Q^a sequence in the Fourier sums, then

$$\frac{1}{N^2}\sum_{Q}\frac{L(\cos Q_x,\cos Q_y)}{\cos\left(\frac{P_x}{2}\right)[1-\cos(Q_x)]+\cos\left(\frac{P_y}{2}\right)[1-\cos(Q_y)]}\rightarrow\frac{1}{\pi^2}\int\int\frac{L(\cos Q_x,\cos Q_y)dQ_xdQ_y}{\cos\left(\frac{P_x}{2}\right)[1-\cos(Q_x)]+\cos\left(\frac{P_y}{2}\right)[1-\cos(Q_y)]}$$

$$\sim\frac{\ln N}{\pi\sqrt{\cos\left(\frac{P_x}{2}\right)\cos\left(\frac{P_y}{2}\right)}}, \tag{15}$$

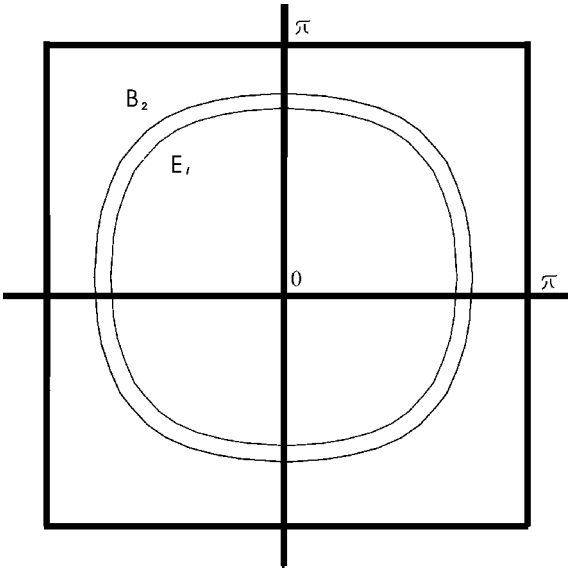

FIG. 3. Critical lines defining the regions of stability (area outside the respective line) for the B_2 mode and the low energy branch of the E mode at $N=40$.

where L is a polynomial. Thus our approach predicts the existence of the logarithmic size dependence for the modes which have at least one ''odd-symmetry'' component. This is illustrated by Fig. 3, containing the critical lines for the B_2 and E^l modes at some mesoscopic values of N. The energy of these modes ''sweeps'' the whole space between the group of three high energy branches and the lowest energy mode A_1 by increasing the number of spins in the system. At mesoscopic values of N they are ''half-way'' between the two limits and could be easily observed. We have also carried out numerical calculations for the discrete lattice at several values of N. Convergence of numerical data with N confirms that the leading term [Eq. (15)] indeed corresponds to the exact asymptotic expansion of the lattice model and the discrepancy is due to higher order corrections. For example, Eq. (14) predicts for the B_2 mode $p_c=2$ for $N=60$ and $p_c=1.86$ for $N=100$, while numerically we find $p_c=1.61$ for $N=60$ and $p_c=1.54$ for $N=100$. Additional confirmation for this behavior comes from our exact results on the lattice model (to be published elsewhere).

Another relevant aspect is the direct relation of the angular dependence of the wave function to the energy of the excitation, which is a general feature of quantum mechanics and is easy to understand. All the low energy modes are characterized by a more ''smooth'' behavior compared to the high energy ones containing more node lines or depleted areas. This point is illustrated by Figs. 4 and 5 showing the behavior of the amplitudes E^l and E^h on a finite lattice for the momenta chosen in the respective regions of stability. These amplitudes correspond to the two branches of the same component (y in the given example) of the E mode. Figure 6 illustrates the oscillating behavior of the E^l amplitude as continued beyond the critical point at $p \leq p_c$. Note that in this region the continuum treatment has to take into account the dense energy spacing of scattering solutions as mentioned above.

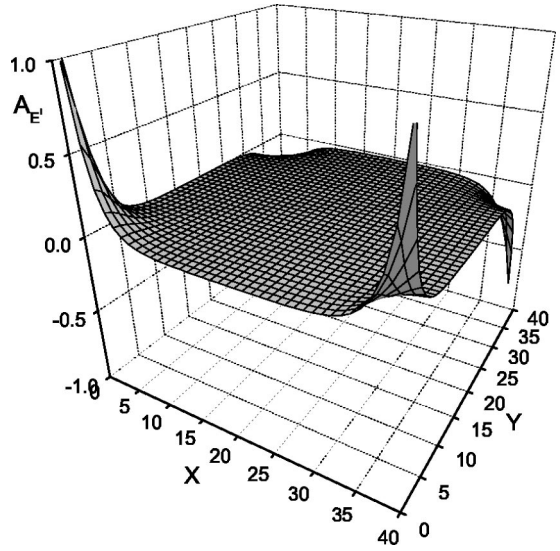

FIG. 4. The low energy branch E^l of the y component of the E mode at $N=40$ for the momentum $p_x=p_y=p \geq p_c$. The critical momentum is determined by Eq. (14).

IV. DISCUSSION

We have considered the features arising in the two-magnon bound states spectra of a finite size ferromagnet within a refined continuum approach. The approach incorporates the symmetry dependent behavior of the underlying discrete lattice and predicts large finite size corrections due to the long wavelength Goldstone singularity of the magnon spectra. We find several new modes and describe the distribution of bound states in the Brillouin zone. It is shown that these modes occupy an even larger area than the known ones, and are therefore important for the low energy spectrum of the Heisenberg ferromagnet. In particular we have noticed a slow convergence of these low energy antisymmetric excitations to the thermodynamic limit. However, one can

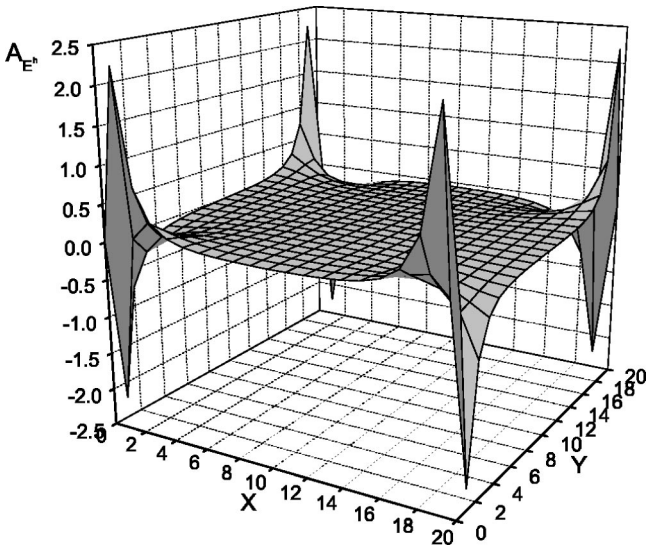

FIG. 5. The high energy branch E^h of the y component of the E mode at $N=40$ for the momentum $p \geq p_c=2 \arccos(4/\pi-1)$.

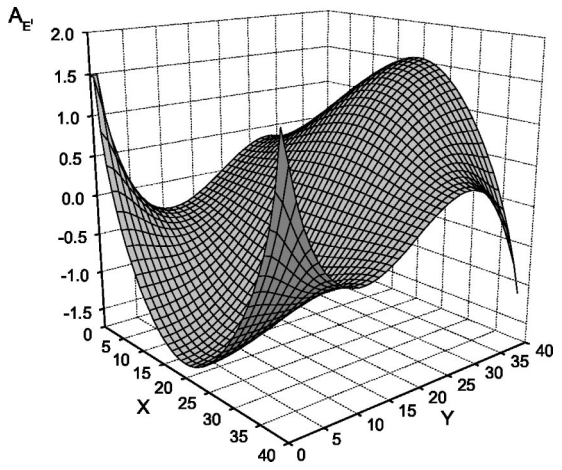

FIG. 6. The low energy branch E^l at $N=20$ as continued for the momentum below the critical point $p_x=p_y=p\leqslant p_c$ in Eq. (14), where it has dissociated into a scattered two-magnon state.

easily see that similar logarithmic size corrections are present in the two-magnon spectra of scattering states. More generally, the same features should also appear in multimagnon spectra, which can be described in terms of the wave function of the form of Eq. (1) with the decoupled motion of the center of mass and relative coordinates. The latter are expressed in terms of the Q ''momenta'' in Eqs. (4) and (5) with shifted sequences of allowed values containing multiples of N in the denominator. This is easy to understand, since an excitation with a fixed total momentum **P** can be viewed as a convolution of multimagnon elementary excitations complying with the boundary conditions in analogy to Eq. (3). By applying our continuum procedure we will recover the same logarithmic behavior, but now due to the ''renormalized'' shifts mentioned above. Conversely, the finite-size behavior of the symmetric modes, such as A_1 or B_1, or some of the antisymmetric modes, such as A_2 or E^h, does not differ much from the thermodynamic limit. In this sense, the present paper reveals the microscopic mechanism of the appearance of logarithmic size-dependent singularities in the thermodynamics of a 2D finite ferromagnet. The stability of the low energy modes increases by increasing the number of spins. At mesoscopic values of N they are well separated from the known ones and can be easily observed. We note that such a behavior is difficult to capture in numerical simulations which are confined to systems of small size. Then even detecting the difference between bound and scattered states causes problems since the wavelength becomes comparable to the size of the system. Thus our explicit results will be useful for the interpretation of numerical simulations. The presented approach can also be extended to other spin or orbital as well as bosonic or fermionic finite size systems.

ACKNOWLEDGMENTS

Financial support from the Concerted Action Scheme of the Flemish Government and from the Belgian National Science Foundation (FWO) is gratefully acknowledged.

APPENDIX A: SYMMETRY ANALYSIS

Our aim is to classify the eigenstates of Eq. (2) according to their transformation properties, i.e., the irreducible representations of the group C_{4v}. Its operations $\hat{G}=\{\hat{I},\hat{C}_4,\hat{C}_4^{-1},\hat{C}_2,\hat{\sigma}_v^x,\hat{\sigma}_v^y,\hat{\sigma}_d^1,\hat{\sigma}_d^2\}$ are mapping amplitude (1) at one lattice point in the space of relative coordinates into another. By our convention of numbering the lattice sites they are defined as follows: $\hat{C}_4 a(P_x,P_y|X,Y)=a(P_y,-P_x|N-Y,X)$, $\hat{\sigma}_v^x a(P_x,P_y|X,Y)=a(P_x,-P_y|X,N-Y)$, $\hat{\sigma}_d^1 a(P_x,P_y|X,Y)=a(P_y,P_x|Y,X)$, etc. We have taken into account that the momentum is transformed by the inverse operations. The projection operator of the νth irreducible representation $\hat{O}^\nu\sim[\Sigma_{\hat{G}}\chi^\nu(\hat{G})\hat{G}]$ acting on each side of (2) projects out the respective eigenmode $A_\nu(P_x,P_y|X,Y)$. Let us now consider the projection onto the B_2 irreducible representation as an example. Then the projection operator generates the combination

$$\begin{aligned}&a(P_x,P_y|X,Y)-a(P_x,P_y|X,N-Y)\\&\quad-a(P_x,P_y|N-X,Y)+a(P_x,P_y|N-X,N-Y)\\&\quad-a(P_y,P_x|N-Y,X)-a(P_y,P_x|Y,N-X)\\&\quad+a(P_y,P_x|Y,X)+a(P_y,P_x|N-Y,N-X),\end{aligned}$$

where we have used the properties $a(P_x,-P_y|X,Y)=a(P_x,P_y|X,Y)=a(-P_x,P_y|X,Y)=$etc. After the projection the amplitude satisfies the symmetry relations specific to this representation:

$$\begin{aligned}A_{B_2}(P_x,P_y|X,Y)=-A_{B_2}(P_x,P_y|X,N-Y)=A_{B_2}(P_x,P_y|N\\-X,N-Y)=-A_{B_2}(P_y,P_x|Y,N-X).\end{aligned}$$

These relations can be checked by substitution, e.g.,

$$\begin{aligned}&A_{B_2}(P_x,P_y|X,N-Y)\\&\quad=a(P_x,P_y|X,N-Y)-a(P_x,P_y|X,Y)\\&\qquad-a(P_x,P_y|N-X,N-Y)+a(P_x,P_y|N-X,Y)\\&\qquad-a(P_y,P_x|Y,X)-a(P_y,P_x|N-Y,N-X)\\&\qquad+a(P_y,P_x|N-Y,X)+a(P_y,P_x|Y,N-X).\end{aligned}$$

The periodic boundary conditions require that this amplitude satisfies the relations in Eq.(3). It then follows that for the B_2 mode both quantum numbers of the total momentum should be odd integers and the Fourier amplitude in Eq. (4) has the property

$$b_{B_2}(P_x,P_y|Q_x,Q_y)=b_{B_2}(P_y,P_x|Q_y,Q_x).$$

The remaining one dimensional representations are obtained in a similar way. For the two components of the E mode we find

$$A_E^y(P_x,P_y|X,Y) = -a(P_y,P_x|Y,N-X) + a(P_y,P_x|N - Y,X) + a(P_y,P_x|Y,X) - a(P_y,P_x|N-Y,N-X);$$

$$A_E^x(P_x,P_y|X,Y) = a(P_x,P_y|X,Y) - a(P_x,P_y|N-X,N-Y) - a(P_x,P_y|X,N-Y) + a(P_x,P_y|N-X,Y).$$

The respective symmetry relations

$$A_E^y(X,Y) = -A_E^y(X,N-Y) = A_E^y(N-X,Y),$$

$$A_E^x(X,Y) = A_E^x(X,N-Y) = -A_E^x(N-X,Y)$$

require that Q_x be even and Q_y odd for the y component, and the reverse for the x component.

APPENDIX B: ASYMPTOTIC EXPANSION

Let us consider the asymptotic expansion corresponding to the discrete sum ($a \equiv \pi/N$)

$$\frac{1}{N^2}\sum_{Q_x^a,Q_y^a} \frac{1}{2-\cos\left(\frac{P}{2}\right)[\cos(Q_x^a)+\cos(Q_y^a)]-\varepsilon/2} \to \int_a^{\pi+a}\int_a^{\pi+a} \frac{1}{2-\cos\left(\frac{p}{2}\right)[\cos(Q_x)+\cos(Q_y)]-\varepsilon/2} \times \frac{dQ_x}{\pi}\frac{dQ_y}{\pi},$$

at the crossing point with the lower boundary of magnon continuum E_L: $\varepsilon/2 = 2[1-\cos(p/2)]$. As we are interested only in the first couple of terms of the expansion the upper limit shift can be neglected. Indeed,

$$\int_\pi^{\pi+a} \frac{1}{2-\cos(Q_x)-\cos(Q_y)}\frac{dQ_x}{\pi} = \frac{-2\arctan\left(\cot\left(\frac{a}{2}\right)\frac{1-\cos Q_y}{\sqrt{(2-\cos Q_y)^2-1}}\right)+\pi}{\pi\sqrt{(2-\cos Q_y)^2-1}} = \frac{a}{3-\cos(Q_x)}+\cdots.$$

Then the first integration gives

$$\int_a^\pi \frac{1}{2-\cos(Q_x)-\cos(Q_y)}\frac{dQ_x}{\pi} = \frac{\frac{2}{\pi}\arctan\left(\cot\left(\frac{a}{2}\right)\frac{1-\cos Q_y}{\sqrt{(2-\cos Q_y)^2-1}}\right)}{\sqrt{(2-\cos Q_y)^2-1}}.$$

On the integration interval we have

$$\cot\left(\frac{a}{2}\right)\frac{1-\cos Q_y}{\sqrt{(2-\cos Q_y)^2-1}} \geqslant 1.$$

Using the expansion

$$\arctan(z) = \frac{\pi}{2} - \frac{1}{z} + \frac{1}{3z^3} - \frac{1}{5z^3} + \cdots,$$

we obtain

$$\frac{\frac{2}{\pi}\arctan\left(\cot\left(\frac{a}{2}\right)\frac{1-\cos Q_y}{\sqrt{(2-\cos Q_y)^2-1}}\right)}{\sqrt{(2-\cos Q_y)^2-1}} = \frac{1}{\sqrt{(2-\cos Q_y)^2-1}} \times\left(1+\frac{2}{\pi}\sum_{k=0}^{\infty}\frac{(-1)^{k+1}}{2k+1}\tanh^{(2k+1)}\left(\frac{a}{2}\right) \times\left(\frac{\sqrt{(2-\cos Q_y)^2-1}}{1-\cos Q_y}\right)^{2k+1}\right).$$

Then integration of the first term gives

$$\left(-\frac{\ln a}{\pi}+\frac{3}{2\pi}\ln 2\right)+\frac{1}{24\pi}a^2+\cdots.$$

The terms of the remaining series can be estimated as

$$\frac{2}{\pi^2}\sum_{k=0}^{\infty}\tanh^{2k+1}\left(\frac{a}{2}\right)\frac{(-1)^{k+1}}{(2k+1)}g_k(a)$$

where

$$g_k(a) = \int_a^\pi \left(\frac{\sqrt{(2-\cos Q_y)^2-1}}{1-\cos Q_y}\right)^{2k+1}\frac{dQ_y}{\sqrt{(2-\cos Q_y)^2-1}}.$$

We are interested in the most singular terms in $g_k(a)$ arising from the singularity of the integrand at $Q_y \sim a$, where we can use the Taylor expansion in Q_y. This leads to the estimate

$$g_k(a) = 2^{2k+1}\int_a^\pi \frac{dy}{y^{2(k+1)}} + O\left(\int_a^\pi \frac{dy}{y^{2k+1}}\right)$$

or

$$g_k(a) \simeq \left(\frac{2}{a}\right)^{2k+1}\frac{1}{(2k+1)}.$$

Using the definition of the Catalan constant

$$C = \sum_{k=0}^{\infty}\frac{(-1)^k}{(2k+1)^2} \simeq 0.915966,$$

for the first two terms of the asymptotic expansion we can finally write

$$\int_{\pi/N}^{\pi+\pi/N}\int_{\pi/N}^{\pi+\pi/N}\frac{1}{2-\cos(Q_x)-\cos(Q_y)}\frac{dQ_y}{\pi}\frac{dQ_x}{\pi}\simeq\frac{1}{\pi}\ln N+\left(\frac{3}{2\pi}\ln 2-\frac{1}{\pi}\ln\pi-\frac{2}{\pi^2}C\right)=\frac{1}{\pi}\ln N-0.219.$$

The respective expansions for the functions in Eq. (13) are obtained in a similar way:

$$A(p)=\frac{1}{\cos(p/2)}\left[\frac{1}{\pi}\ln\left(\frac{N}{\pi}\right)+\frac{3}{2\pi}\ln 2-\frac{2}{\pi^2}C-\frac{1}{2}\right]+O(1/N),$$

$$B(p)=\frac{1}{\cos(p/2)}\left[\frac{1}{\pi}\ln\left(\frac{N}{\pi}\right)+\frac{3}{2\pi}\ln 2-\frac{2}{\pi^2}C-1+\frac{2}{\pi}\right]+O(1/N),$$

$$C(p)=\frac{1}{\cos(p/2)}\left[\frac{1}{\pi}\ln\left(\frac{N}{\pi}\right)+\frac{3}{2\pi}\ln 2-\frac{2}{\pi^2}C-\frac{2}{\pi}\right]+O(1/N).$$

It is also not difficult to find the main term of the asymptotic expansion for an arbitrary direction in the Brillouin zone [Eq. (15)]. Indeed, let us consider the integral

$$\frac{1}{\pi^2}\int\int\frac{\cos^k(Q_x)\cos^m(Q_y)dQ_xdQ_y}{\cos\left(\frac{P_x}{2}\right)[1-\cos(Q_x)]+\cos\left(\frac{P_y}{2}\right)[1-\cos(Q_y)]}$$

where m and k are arbitrary integers and at least one of the integration limits contains the cut-off a; both $\cos(P_x/2)$ and $\cos(P_y/2)$ are considered to be positive. By keeping only the main terms after the first integration we obtain (below b is either 0 or a)

$$\int_b^{\pi}\frac{\cos^m(Q_y)}{\cos\left(\frac{P_x}{2}\right)[1-\cos(Q_x)]+\cos\left(\frac{P_y}{2}\right)[1-\cos(Q_y)]}\frac{dQ_y}{\pi}\simeq\frac{\left(1+\frac{\cos\left(\frac{P_x}{2}\right)}{\cos\left(\frac{P_y}{2}\right)}[1-\cos(Q_x)]\right)^m}{\sqrt{\cos\left(\frac{P_x}{2}\right)[1-\cos(Q_x)]+2\cos\left(\frac{P_y}{2}\right)}}\times\frac{1}{\sqrt{\cos\left(\frac{P_x}{2}\right)[1-\cos(Q_x)]}}.$$

In the second integration we may put $Q_x=0$ in the prefactor of the singular term above. Thus we obtain

$$\frac{1}{\pi}\frac{1}{\sqrt{2\cos\left(\frac{P_x}{2}\right)\cos\left(\frac{P_y}{2}\right)}}\int_a^{\pi}\frac{\cos^kQ_x}{\sqrt{1-\cos Q_x}}dQ_x\simeq-\frac{1}{\pi}\frac{1}{\sqrt{\cos\left(\frac{P_x}{2}\right)\cos\left(\frac{P_x}{2}\right)}}\ln a.$$

*On leave from the Institute of Applied Physics, Chişinău, Moldova.

[1] For spin effects in mesoscopic systems, see Solid State Commun. **119**, 181 (2001).

[2] J. Brooke, T.F. Rosenbaum, and G. Aeppli, Nature (London) **413**, 610 (2001).

[3] W. Belzig, A. Brataas, Y.V. Nazarov, and G.E.W. Bauer, Phys. Rev. B **62**, 9726 (2000).

[4] H. Mathur, Phys. Rev. Lett. **78**, 2429 (1997).

[5] R. Sessoli, D. Gateschi, A. Caneschi, and M.A. Novak, Nature (London) **365**, 141 (1993).

[6] H. Bethe, Z. Phys. **71**, 205 (1931).

[7] D. C. Mattis, *The Theory of Magnetism* (Springer-Verlag, Berlin, 1981), Vol. I, p. 300.

[8] A. Ceulemans, S. Cojocaru, and L.F. Chibotaru, Eur. Phys. J. B **21**, 511 (2001).

[9] N. Fukuda and M. Wortis, J. Phys. Chem. Solids **24**, 1675 (1963).

[10] M. Wortis, Phys. Rev. **132**, 85 (1963).

[11] M. Hood and P.D. Loly, J. Phys. C **19**, 4729 (1986).

[12] Yu. A. Izyumov, Yu. N. Skriabin, and R. Cooker, *Statistical Mechanics of Magnetically Ordered Systems* (Consultants Bureau, New York, 1988), p. 295.

[13] R.G. Boyd and J. Callaway, Phys. Rev. **138**, A1621 (1965).

[14] F. Woynarovich, J. Phys. A **15**, 2985 (1982).

[15] A.A. Vladimirov, Phys. Lett. A **105**, 418 (1984).

[16] D. Richards, *Advanced Mathematical Methods* (Cambridge University Press, Cambridge, 2002), p. 149.

[17] J.P. Elliot and P.G. Dawber, *Symmetry in Physics* (Macmillan, London, 1979), Vol. I, p. 360.